

Study of graphitic microstructure formation in diamond bulk by pulsed Bessel beam laser writing

S. Kumar¹ · B. Sotillo² · A. Chiappini³ · R. Ramponi² · P. Di Trapani¹ · S. M. Eaton² · O. Jedrkiewicz⁴

Received: 28 July 2017 / Accepted: 6 October 2017 / Published online: 19 October 2017
© Springer-Verlag GmbH Germany 2017

Abstract The advantages of using Bessel beams for the generation of graphitic structures in diamond bulk are presented. We show that by irradiating the sample with a pulsed Bessel beam whose non-diffracting zone is of the same order of the sample thickness, it is possible to produce without any sample translation straight graphitic through-microstructures, whose size depends on the input pulse energy. The microstructure growth is investigated as a function of the number of irradiating pulses, and the femtosecond and picosecond regimes are contrasted.

1 Introduction

Diamond is a remarkable material which, thanks to its exceptional properties, is finding application in many new technologies [1], including for instance integrated optics [2, 3], quantum information systems [4, 5] and microfluidics [6]. Diamond is transparent at near-infrared wavelengths, however a tightly focused pulsed laser beam can undergo multiphoton absorption and, at intensities above a threshold, induces a highly localized breakdown of the diamond lattice [7]. The possibility to generate graphitic structures inside

the diamond bulk by means of laser processing has been thoroughly investigated in the last few years [8–16], especially for various potential applications, such as all-carbon diamond radiation detection [17–19] or metallo-dielectric photonic crystals [8]. To generate homogeneous and uniform graphitic wires, ultrashort pulse durations (in the femtosecond or picosecond regime) should be used to minimize the thermal effects [9, 19]. Moreover, the influence of the sample translation on the generation and growth of the laser-graphitized microstructures in the bulk has been presented in different works [12, 13, 15, 16].

In this paper, we present a study on the spontaneous formation of straight graphitic microstructures inside the bulk of a 500- μm thick synthetic monocrystalline diamond substrate, without the need of sample translation along the beam propagation direction. The elongated microstructuring process covering the whole sample thickness is possible thanks to the use of a pulsed finite energy Bessel beam, featured by a localized intense micron-size central peak and by a non-diffracting focal zone (the so-called Bessel zone) with length comparable to the sample thickness. Bessel beams, whose central core is surrounded by rings that constitute the beam energy reservoir for a non-diffracting propagation, are a particularly interesting class of light beams [20], which can be generated by conical lenses (axicons) or holograms. As we shall see, thanks to this conical flux, which allows the reconstruction of the Bessel central core along the propagation direction, the graphitization at the surface of the sample by the first pulse does not block the irradiation effect inside the bulk of subsequent pulses. We focus our attention on the characteristics of the resulting microstructures and their interesting growth dynamics from the bottom surface to the top surface of the sample. We analyze their features dependence on the pulse energy, the number of irradiating pulses and the pulse duration. We show that for higher energies the

✉ O. Jedrkiewicz
ottavia.jedrkiewicz@ifn.cnr.it

¹ Dipartimento di Scienza e Alta Tecnologia, Università degli Studi dell'Insubria, Via Valleggio 11, 22100 Como, Italy

² CNR, Istituto di Fotonica e Nanotecnologie, and Politecnico di Milano, Piazza Leonardo da Vinci 32, 20133 Milano, Italy

³ CNR, Istituto di Fotonica e Nanotecnologie, CSMO lab., Via alla Cascata 56/C, 38123 Povo, Trento, Italy

⁴ CNR, Istituto di Fotonica e Nanotecnologie, Udr di Como, Via Valleggio 11, 22100 Como, Italy

graphitic structures grow faster, however the use of lower energies allows to generate thinner and more homogeneous wires. The laser-graphitized tracks are also shown to grow faster when, for a given energy, picosecond instead of femtosecond pulses are used.

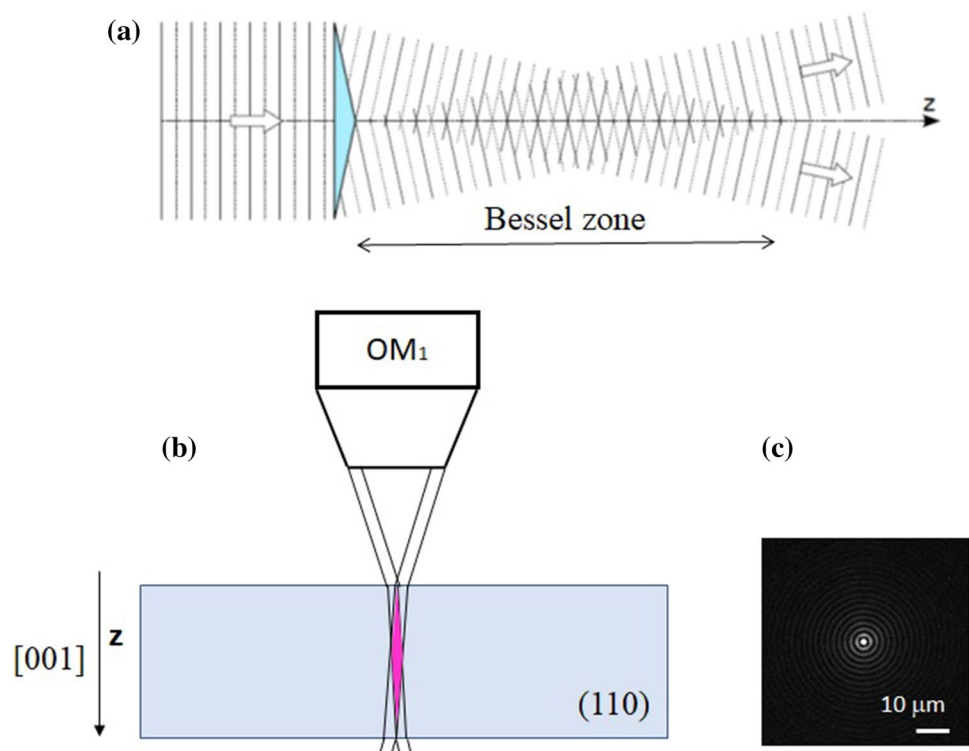
2 Experimental set-up

The experiment was performed by means of a 20 Hz Ti:sapphire laser system (Amplitude Technologies) delivering 40 fs transform-limited pulses at 800 nm wavelength. As already observed, the use of a low repetition rate laser source enhances the formation of nanocrystalline graphite with respect to amorphous carbon [2, 6]. By detuning the laser compressor, the pulse could be stretched and the pulse duration adjusted. The Gaussian laser beam was spatially filtered and demagnified before being reflected onto a spatial light modulator (SLM, Holoeye) for the generation of the Bessel beam (BB). The SLM imprints on the beam, the phase mask of a conical lens (axicon), with parameters to have a Bessel beam featured by a 20° cone angle in air. As shown in the experimental set-up reported in [6, 21], the BB was then demagnified by a suitable telescopic system constituted by a $f=300$ mm lens (L_1) and a 0.45 N.A. $20\times$ optical microscope objective (OM_1),

before being injected orthogonally to the (001)-oriented surface of a polished synthetic monocrystalline diamond sample (type II, $7\times 7\times 0.5$ mm³, MB Optics). During the laser writing, a real-time imaging onto a CCD camera of the (back-illuminated) sample, was realized by means of a telescopic system constituted by the microscope objective OM_1 and a 150-mm lens (L_2).

Before microfabrication, the Bessel beam was characterized in air by means of an imaging system, highlighting in the transverse profile a central core size of $0.7\ \mu\text{m}$ evaluated as full width at half maximum (FWHM) and a total non-diffracting zone length along z of about $250\ \mu\text{m}$. For the optimization of the graphitized microstructure generation, the relative positioning of the BB with respect to the sample thickness was carefully adjusted taking into account that the intensity profile of a finite energy BB is not flat along the propagation direction [22], and depends on the radial energy distribution of the apodized Gaussian beam profile impinging on the SLM. The high refractive index of diamond ($n=2.4$) ensures a further elongation of the BB inside the diamond bulk guaranteeing the intensity distribution of the non-diffracting zone across the whole sample thickness. In Fig. 1, we present to illustrate the Bessel beam formation as a result of the interference of the refracted rays through an axicon together with a scheme of the relative positioning between the Bessel zone and the sample.

Fig. 1 **a** Example of BB formation: in our experiment, the BB was in fact generated by an SLM imprinting on to the beam, the phase profile of an axicon; **b** scheme of the relative positioning of the Bessel zone with respect to the sample. **c** Transverse intensity profile of the BB used during laser processing



3 Results and discussion

Typical traces left on the diamond sample surface after single-shot Bessel beam irradiation are presented in Fig. 2 for illustration. The modifications shown in the optical microscope images of Fig. 2 have been obtained with a 200-fs (top row) and 2-ps (bottom row) pulse duration, and in each of these regimes with two different laser pulse energy values, to work with fluences associated with the BB central core (around few J/cm^2) above the diamond damage threshold [23].

In this single-shot machining regime, even if the material modification is evident on the surface, when looking at the sample from the lateral side under the optical microscope, no evident refractive index change or ablation traces inside the bulk could be detected, in contrast to the case of glass [21]. Nevertheless, it is possible to generate graphitized high aspect-ratio through-structures when working in multiple shot regime. The fabrication of graphitic microstructures has been performed in different experimental conditions, by varying the energy and the exposure time. Two different pulse durations have been taken into account, for a comparison of the growth dynamics in the femtosecond (fs) and in the picosecond (ps) regime.

Figure 3 shows optical microscope images of arrays of microstructures written close to a polished side of the diamond sample, along its 500- μm thickness, in two different pulse energy conditions; 3.5 and 10 μJ for the fs pulses,

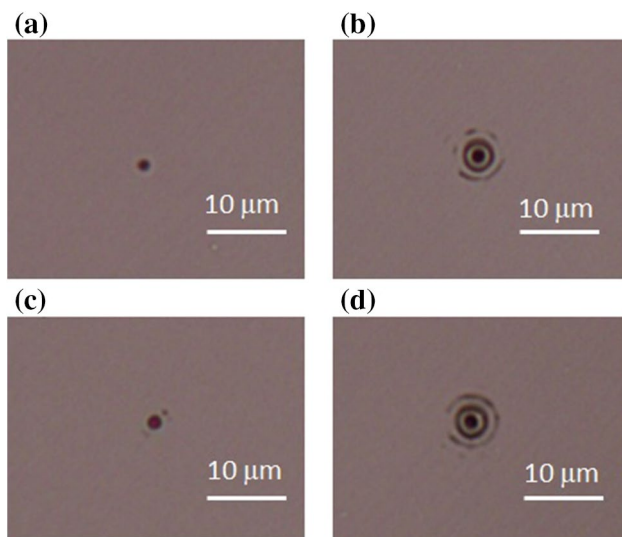


Fig. 2 Optical microscope images of typical single-shot traces left by the Bessel beam on the diamond sample surface in different energy conditions, and for two pulse durations; 200 fs (top row) and 2 ps (bottom row). The energy per pulse used in the two regimes was 3.5 μJ (a), 10 μJ (b), and 5 μJ (c), 10 μJ (d), respectively. Note that in the fs and in the ps regimes, no evident trace on the top surface appears if the energy per pulse lies below 3.5 and 5 μJ , respectively

and 5 μJ and 10 μJ for the ps pulses. Note that in the latter case, we have arbitrarily chosen an energy of 5 μJ instead of 3.5 μJ , so to observe a graphitic trace left by the Bessel beam irradiation on the top surface similar to the fs case (as also illustrated in Fig. 2a, c), and thus to work in similar initial writing conditions. The exposure time, expressed here in terms of the number of irradiating pulses, has been varied as indicated at the bottom of each image. The relative position between the Bessel beam and the sample was fixed in all cases. The growth of the graphitized microtracks could be observed in real-time and it always occurred from the bottom surface towards the top surface, and thus in the opposite direction with respect to the BB propagation direction. Despite the fact that the focusing geometry is clearly different here, this seems to be in analogy with previous observation where with continuous irradiation from a focused Gaussian laser pulse the graphitized region tends to grow towards the incident laser beam [12]. Moreover, although the central core fluence in our experiment is generally higher in the middle of the diamond sample because of the redistribution of the energy along the non-diffracting zone, we believe that the fact that the phase transition is always initiated at the crystal faces (in particular from the bottom towards the top) may be explained by a lower graphitization threshold at the rear surface with respect to that in the bulk [11, 12, 24]. Multiple shot irradiation of the diamond bulk after the optical breakdown causes the extension of a continuous graphitized region as propagation of the “graphitization” wave [25]. This occurs due to the heat diffusion from the light-absorbing modified region, and is favored in this case by the elongated focal line of the Bessel beam which is expected to enhance the multiphoton ionization.

One can notice from Fig. 3 that the length of the graphitized microstructures varies with the exposure time (increases for a larger number of irradiating pulses), and the homogeneity of these microstructures is strongly dependent on the energy. On the other hand for a given pulse energy, there seems to be a minimum exposure time for which it is possible to generate visible dark tracks inside the diamond bulk. We recognize especially in the high energy case feather-like structures as those already reported [12, 13, 26], whose geometry depends on the crystallographic direction along which the structure is growing. Indeed, we confirm boundaries of these substructures at an angle of about 54° corresponding to the angle between the (001) and (111) crystal plane.

In the femtosecond regime, when irradiating the sample with more than 2000 pulses, we also notice that additional graphitized lines departing from the main channel-like structure appear in the higher energy case. We have observed that the angle of these with respect to the propagation direction forms approximately 8° , this value being compatible with the Bessel beam cone angle inside the bulk. This may

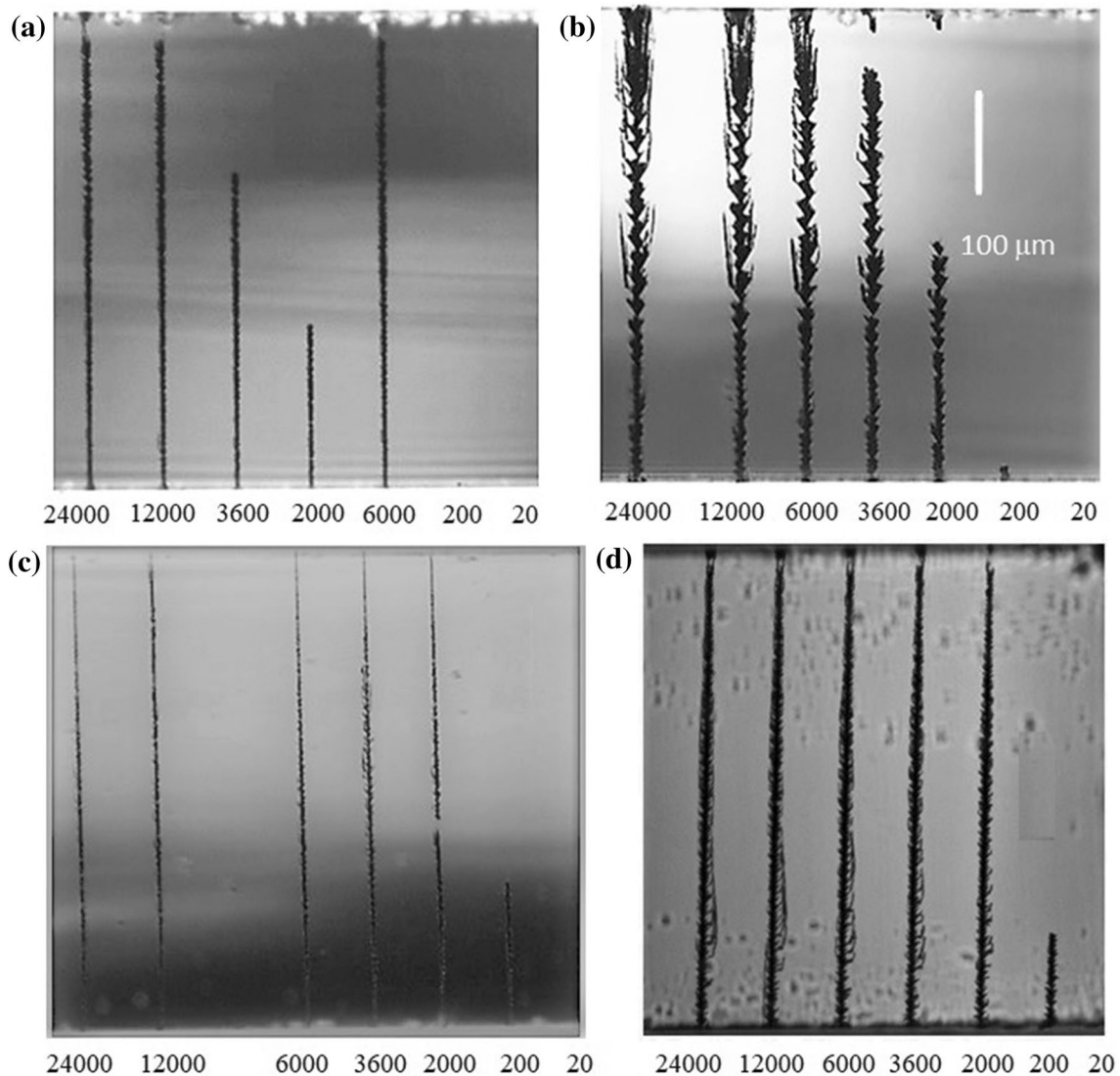


Fig. 3 Optical microscope images (side view) of arrays of graphitized microstructures fabricated by BB in the diamond bulk without axial sample translation, for different numbers of irradiating pulses (indicated below each trace). Top and bottom of each image correspond to top and bottom surfaces, respectively. Pulses of 200 fs (top row) and 2 ps (bottom row) duration have been used. The energy

per pulse used in the two regimes was 3.5 μJ (a), 10 μJ (b), and 5 μJ (c), 10 μJ (d), respectively. Note that the tracks in a, b, c have been written on a sample side which was opposite to an accidentally damaged side. This explains the presence of shadows on the images recorded with the transmission microscope. The scale bar is the same for all the microscope images and corresponds to 100 μm

indicate the influence of the high intensity beam used, and the effect on the material modification coming not only from the central BB core, but also from the conical energy reservoir in the form of the few first surrounding rings (whose traces also are evident in Fig. 2b, d).

When using picosecond pulses, additional weaker graphite filaments seem to appear around the main channel-like tracks, which in turn seem generally more homogeneous than those written with femtosecond pulses. However in the higher energy case, we notice that these graphitic microstructures are not well connected with the top surface traces (as visible in Fig. 3c, d). Finally, we observe that for a given

laser pulse energy the width of the generated tracks is independent on the exposure time.

The evolution of the microstructure length as a function of the number of irradiating pulses is presented in Fig. 4. Note that the repeatability of the results was tested and verified, and we observed that given a fixed number of shots, the length of the graphitic structures varied at most within 10 μm (i.e. within the square size of the data points plotted in Fig. 4). In the femtosecond regime, it is clear that the use of higher pulse energy leads to a faster growth. Note in both cases, a saturation effect due to the finite sample thickness was observed. In fact, arbitrary graphitic wires lengths are

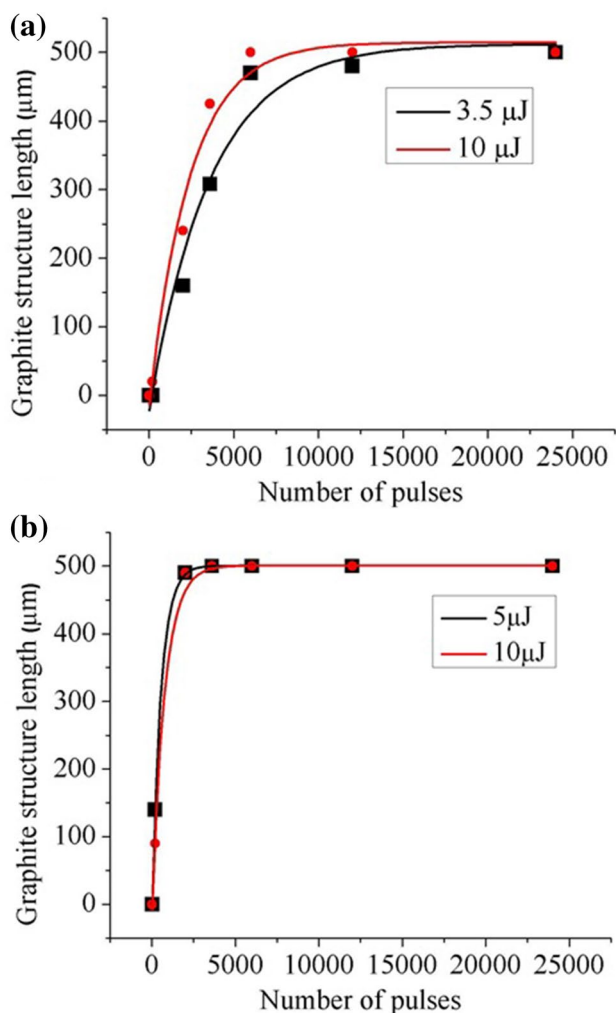


Fig. 4 Graphs of the microstructures length plotted as a function of the number of irradiating pulses, in the two experimental conditions: **a** femtosecond and **b** picosecond irradiation, in each case for the two pulse energy values considered

obtainable depending on the Bessel beam geometry; for a through-microstructure, the condition is that the Bessel zone length in the bulk has to be of the same order of the sample thickness.

By comparing the experimental results reported in Fig. 4a, b, it appears that using pulsed Bessel beams in the picosecond regime produces faster growing graphitic microwires, than in the femtosecond regime. We believe that this enhancement effect is favored by the presence on such time scales of the avalanche ionization process [21, 27].

We have also estimated that the growth rate of the graphitic tracks generated by means of Bessel beams is higher than in standard irradiation situations (where, moreover, the sample must be translated for optimum generation conditions). Focusing our attention on the lower energy irradiation conditions, for which we have homogeneously thin

graphitized microwires, and considering that in the femtosecond case, these wires reach 400 μm length with about 5000 pulses; this means that the corresponding growth rate for a 1 kHz laser source, would be 80 μm/s, that is from three times up to almost one order of magnitude higher than what was reported in [12]. On the other hand for the picosecond case, where the graphitic lines grow even faster and reach 500 μm after 3600 irradiating pulses, we can estimate a growth rate of more than 1.2 mm/s in the hypothesis of using a 10 kHz laser source or 6 mm/s in the hypothesis of using a 50 kHz laser source, so in both cases higher than what was reported in [13], where they reached, respectively, 260 μm/s and 4 mm/s. The model for laser-induced graphitization of diamond bulk developed by Kononenko et al. [11, 25] based on the optical breakdown and the propagation of the graphitization wave can be applied to our experiments. The small discrepancy observed here is attributed to the use of a Bessel beam, which propagates along the focal line thanks to the continuous refilling of energy arriving from its conical reservoir, i.e. the surrounding rings. The presence of an extended focus crossing the whole sample thickness may enhance the wave propagation process and lead to a slightly higher growth rate. We may see here the irradiation system as an ensemble of simultaneous focal points distributed along a line that may contribute to the increase of the graphitization wave speed thanks to the increased efficiency of diamond ionization and plasma-assisted energy absorption along the sample thickness.

As mentioned before, there is a difference in terms of width homogeneity along the sample thickness when considering fs or ps pulses. In the first case, a slight broadening of the tracks width occurs during the spontaneous growth towards the sample top surface. This is already observable in the images of Fig. 3. To verify this hypothesis, we repeated the microfabrication in the two regimes, by varying the pulse energy in a broader range. The results confirm the precedent observation, highlighting also that in the picosecond regime thinner micron-size wires can be fabricated. Figure 5 shows a portion of an array of graphitic microstructures (in the center of the bulk) fabricated by the BB with different pulse energies in the two pulse duration cases. A graph summarizing the behavior of the graphite microstructure width when increasing the laser pulse energy is also presented.

The presence of graphitic-like phase in the formed tracks was verified by examining the microstructural properties of the laser-modified regions through micro-Raman spectroscopy. The spectra were recorded by means of a Labram Aramis John Yvon Horiba system with a DPSS laser source at 532 nm and equipped with a confocal microscope, a 1800 line/mm grating and an air-cooled CCD. The Raman signal was collected in a backscattering configuration with a 100x objective, achieving a spatial resolution of about 1 μm. As an example, we

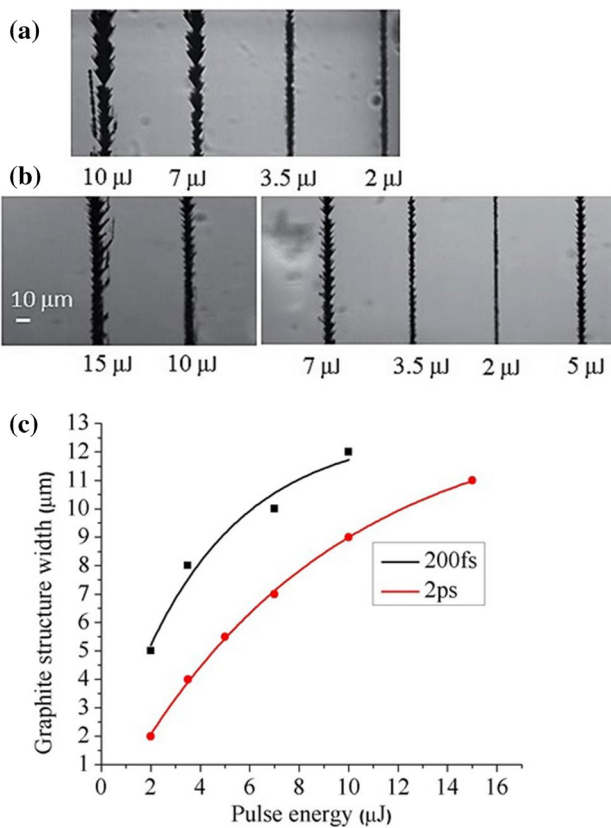


Fig. 5 **a** Zoomed optical microscope image of a central portion of an array of microstructures fabricated by BB at different pulse energies in the fs (**a**) and in the ps (**b**) irradiation regime and **c** corresponding graphs showing the width of the tracks versus the energy used. The width has been estimated by taking into account also the feather-like substructures. The scale bar is the same for all the microscope images and corresponds to 10 μm

present in Fig. 6 the results for one of the tracks shown in Fig. 3b (200 fs, 10 μJ), where the measurements have been performed at different positions along the width of the irradiated region at the sample surface (see Fig. 6a). Note that no strong differences in the Raman spectra features are observed for the different irradiation conditions. Inside the track, we see a decrease in the intensity of the Raman diamond peak at 1332 cm⁻¹, and the appearance of two new peaks centered at 1580 cm⁻¹ (G-peak) and 1345 cm⁻¹ (D-peak). This is related to the transformation of the characteristic sp³ diamond bonding into sp² bondings. Note that the Raman spectra recorded along the length of a trace also have shown the D- and G-peaks. However, the signal of these components is much lower with respect to the 1332 cm⁻¹ peak due to a larger collection of the Raman signal coming from the diamond surrounding the trace, related to the elongation of the

focal volume in depth produced by the spherical aberration. From the position of the G-peak, its width (FWHM below 100 cm⁻¹) and the relative intensity of the D- and G-peaks ($I(D)/I(G)$ of about 1), the carbon phase formed by the laser irradiation is a mixture of amorphous carbon and nanocrystalline graphite, with an estimated crystalline size of 1.5 nm (calculated for the $I(D)/I(G)$ ratio following the formula $I(D)/I(G) = C(\lambda) \cdot L_a^2$, being $C(\lambda)$ a constant that depends on the wavelength and L_a the cluster diameter [28]). The appearance of second-order Raman peaks at 2700 cm⁻¹ (2D peak) and 2900 cm⁻¹ (D + G peak) further supports the formation of ordered graphitic-like phase [28]. The luminescence background observed could be related to damage defects created by the laser. Note also that in all the points checked inside the track, we are still able to detect the diamond-related peak, which suggests that not all the irradiated volume is transformed into the graphitic-phase, as is also observed in Fig. 3b. The intensity ratio between the diamond peak 1332 cm⁻¹ and the G-peak at 1580 cm⁻¹ varies along the width of the structure (Fig. 6c). These observations suggest that we are forming microstructures with similar features to the wires fabricated with femtosecond laser writing and recently reported by Salter et al. [29], where by means of TEM measurements they observed that the transformation of diamond into sp² clusters is not uniform inside the graphitic structures. Nevertheless, the conductivity of those wires is very promising [15], and future work shall be dedicated to the investigation of the resistivity of the microstructures generated by Bessel beams.

4 Conclusions

Bulk microstructuring by means of pulsed Bessel beam irradiation in a synthetic monocrystalline diamond has been studied. We have presented the features of the graphitic microtracks that can be generated without any axial sample translation when the elongated focal zone of the Bessel beam is distributed across the sample thickness, highlighting the differences with previous works, and the advantage in terms of growth rate. We have characterized the length, and thickness of the graphitized microstructures obtained in different experimental conditions, and we have presented their features as function of the pulse duration, number of irradiating pulses, and pulse energy. Provided the latter is suitably chosen above a threshold value for bulk modification, the picosecond Bessel beam micromachining regime is favorable for producing more homogeneous microwires, which can rapidly grow inside the diamond bulk.

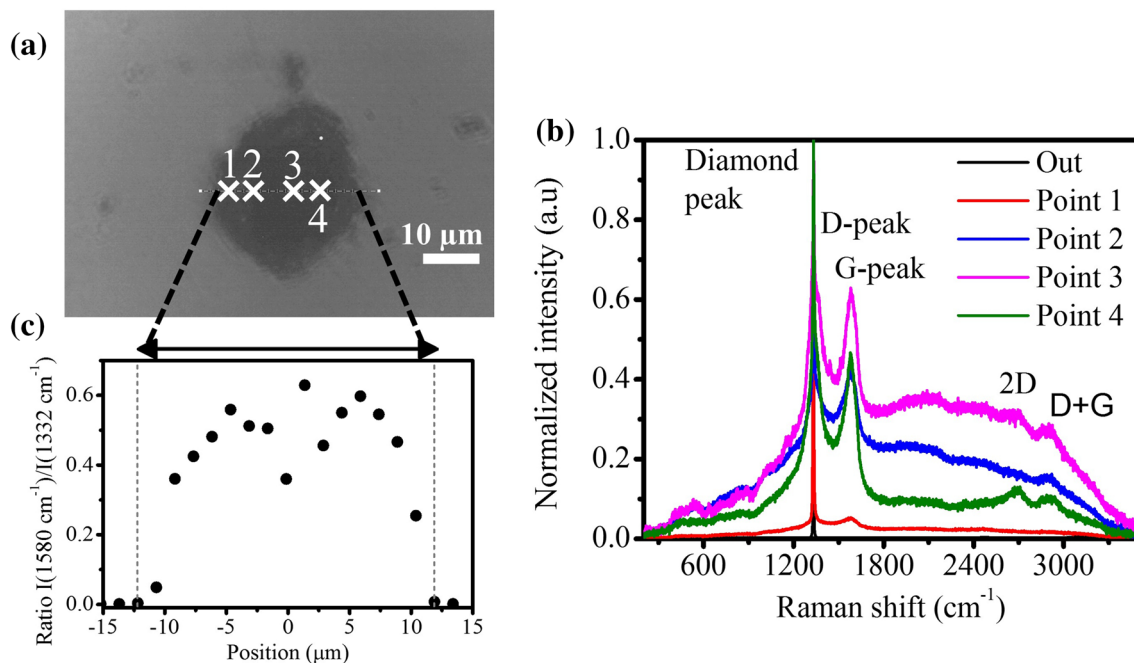


Fig. 6 **a** Optical transmission microscope image (recorded at the top surface of the sample) of a track written by a 200-fs BB (after 24,000 laser pulses, with laser pulse energy of 10 μJ). **b** Micro-Raman spectra

normalized to the diamond Raman peak, and **c** intensity ratio between the G-peak (1580 cm^{-1}) and the diamond peak (1332 cm^{-1}), recorded at different points along the width of the trace

Acknowledgements FP7 Diamond Fab CONCERT Japan project; DIAMANTE MIUR-SIR grant; FemtoDiamante Cariplo ERC reinforcement Grant.

References

- I. Aharonovich, A.D. Greentree, S. Praver, *Nat. Photonics* **5**, 397 (2011)
- B. Sotillo, V. Bharadwaj, J.P. Hadden, M. Sakakura, A. Chiappini, T.F. Fernandez, S. Longhi, O. Jedrkiewicz, Y. Shimotsuma, L. Criante, R. Osellame, G. Galzerano, M. Ferrari, K. Miura, R. Ramponi, P.E. Barklay, S. Eaton, *Sci. Reports* **6**, 35566 (2016)
- A. Courvoisier, M.J. Booth, P. Salter, *Applied Phys. Lett* **109**, 031109 (2016)
- F. Jelezko, J. Wrachtrup, *Phys. Status Solidi (a)* **203**, 3207–3225 (2006)
- D.D. Awschalom, R. Epstein, R. Hanson, *Sci. Am* **297**, 84–91 (2007)
- O. Jedrkiewicz, S. Kumar, B. Sotillo, M. Bollani, A. Chiappini, M. Ferrari, R. Ramponi, P. Di Trapani, S. Eaton, *Opt. Mat. Express* **7**, 290408 (2017)
- I. Konov, *Laser Photonics Rev* **6**, 739 (2012)
- M. Shimizu, Y. Shimotsuma, M. Sakakura, T. Yuasa, H. Homma, Y. Minowa, K. Tanaka, K. Miura, K. Hirao, *Opt. Express* **17**, 46 (2009)
- T.V. Kononenko, M.S. Komlenok, V.P. Pashinin, S.M. Pimenov, V.I. Konov, M. Neff, V. Romano, W. Lüthy, *Diamond Relat. Mater* **18**, 196 (2009)
- T.V. Kononenko, V.I. Konov, S.M. Pimenov, N.M. Rossukanyi, A.I. Rukovichnikov, V. Romano, *Diamond Relat. Mater* **20**, 264 (2011)
- T.V. Kononenko, M. Meier, M.S. Komlenok, V.P. Pashinin, S.M. Pimenov, V.I.V. Romano, V.P. Pashinin, V.I. Konov, *Appl. Phys. A* **90**, 645 (2008)
- M. Neff, T.V. Kononenko, S.M. Pimenov, V. Romano, W. Lüthy, V.I. Konov, *Appl. Phys. A* **97**, 543 (2009)
- S.M. Pimenov, I.I. Vlasov, A.A. Khomich, B. Neuenschwander, M. Mural, V. Romano, *Appl. Phys. A* **105**, 673 (2011)
- T.V. Kononenko, A.A. Khomich, V.I. Konov, *Diamond Relat. Mater* **37**, 50 (2013)
- B. Sun, P.S. Salter, M.J. Booth, *Appl. Phys. Lett.* **105**, 231105 (2014)
- M. Girolami, A. Bellucci, P. Calvani, S. Orlando, V. Valentini, D.M. Trucchi, *Appl. Phys. A* **117**, 143 (2014)
- B. Caylar, M. Pomorsky, P. Bergonzo, *Appl. Phys. Lett.* **103**, 043504 (2013)
- T.V. Kononenko, V. Ralchenko, A. Bolshakov, V. Konov, P. Allegrini, M. Pacilli, G. Conte, E. Spiriti, *Appl. Phys. A* **114**, 297 (2014)
- S. Lagomarsino, M. Bellini, C. Corsi, S. Fanetti, F. Gorelli, I. Lontos, G. Parrini, M. Santoro, S. Sciortino, *Diamond Relat. Mater* **43**, 23 (2014)
- J. Durning, J. Miceli, J.H. Eberly, *Phys. Rev. Lett.* **58**, 1499 (1987)
- V. Garzillo, V. Jukna, A. Couairon, R. Grigutis, P. Di Trapani, O. Jedrkiewicz, *J. of Appl. Phys* **120**, 013102 (2016)
- D. Mc Gloin, K. Dholakia, *Contemp. Phys.* **46**, 15 (2005)
- H.O. Jeschke, M.E. Garcia, *Appl. Surf. Sci* **197–198**, 107–113 (2002)
- N.L. Boling, M.D. Crisp, G. Dube, *Appl. Opt* **12**, 650 (1973)
- T.V. Kononenko, E.V. Zavedeev, V.V. Kononenko, K.K. Ashik-kalieva, V.I. Konov, *Appl. Phys. A* **119**, 405 (2015)
- B. Sun, P.S. Salter, M.J. Booth, *Proc. of SPIE* **9736**, 973612–973611 (2016)
- R.R. Gattass, E. Mazur *Nature Photonics* **2**, 219–225 (2008)
- A.C. Ferrari, J. Robertson, *Phys. Rev. B* **61**, 14095 (2000)
- P.S. Salter, M.J. Booth, A. Courvoisier, D.A. Moran, D.A. MacLaren, *Appl. Phys. Lett.* **111**, 081103 (2017)